BBA - Bioenergetics 1860 (2019) 30–40

Contents lists available at ScienceDirect

BBA - Bioenergetics

journal homepage: www.elsevier.com/locate/bbabio

Redox-state dependent blinking of single photosystem I trimers at around liquid-nitrogen temperature

Sankar Jana[a,1], Ting Du[a], Ryo Nagao[b,2], Takumi Noguchi[b], Yutaka Shibata[a,*]

[a] Department of Chemistry, Graduate School of Science, Tohoku University, Aramaki Aza Aoba, Aoba-ku, Sendai 980-8578, Japan
[b] Division of Material Science (Physics), Graduate School of Science, Nagoya University, Furo-cho, Chikusa-ku, Nagoya 464-8602, Japan

ARTICLE INFO

Keywords:
Single-molecule spectroscopy
Fluorescence blinking
Site energy
Cryogenic microscope
Phylloquinone
Electrochromic shift

ABSTRACT

Efficient light harvesting in a photosynthetic antenna system is disturbed by a ragged and fluctuating energy landscape of the antenna pigments in response to the conformation dynamics of the protein. This situation is especially pronounced in Photosystem I (PSI) containing red shifted chlorophylls (red Chls) with the excitation energy much lower than the primary donor. The present study was conducted to clarify light-harvesting dynamics of PSI isolated from *Synechocystis* sp. PCC6803 by using single-molecule spectroscopy at liquid-nitrogen temperatures. Fluorescence emission at around 720 nm from the red Chls in single PSI trimers was monitored at 80–100 K. Intermittent variations in the emission intensities, so-called blinking, were frequently observed. Its time scale lay in several tens of seconds. The blinking amplitude depended on the redox state of the phylloquinone (A_1). Electrochromic shifts of Chls induced by the negative charge on A_1 were calculated based on the X-ray crystallographic structure. A Chl molecule, Chl-A839 (numbering according to PDB 5OY0), bound near A_1 was found to have a large electrochromic shift. This Chl has strong exciton coupling with neighboring Chl (A838) whose site energy was predicted to be determined by interaction with an arginine residue (ArgF84) [Adolphs et al., 2010]. A possible scenario of the blinking was proposed. Conformational fluctuations of ArgF84 seesaw the excitation-energy of Chl-A838, which perturbs the branching ratio of excitation-energy between the red Chl and the cationic form of P700 as a quencher. The electrochromic shift of Chl-A839 enhances the effect of the conformation dynamics of ArgF84.

1. Introduction

Single-molecule spectroscopy (SMS) has provided a powerful tool to reveal fluctuation dynamics of molecular environment embedding a target molecule of interest. Scientists have continuously expanded the range of application of SMS to many biological systems including photosynthetic systems. Recent SMS studies on photosynthetic antenna systems have clarified that the efficiency of light harvesting fluctuates in time [1–3]. These observations have necessitated updates to a widely held belief that light-harvesting systems in photosynthesis have a high robustness in efficient funneling of light energy to a reaction center. Although SMS studies have uncovered fluctuation in photosynthetic light harvesting, the underlying molecular mechanism has not been well understood yet. The limited robustness of light-harvesting efficiency may be related to the ability of natural photosynthetic systems to regulate energy input to the reaction center in response to environmental changes.

Photosystem I (PSI) is one of two photosystems involved in oxygenic photosynthesis in plants, algae, and cyanobacteria. PSI is a giant pigment-protein complex composed of more than 10 subunits. PSI binds many cofactors including 95–98 chlorophyll (Chl)-*a* molecules, 2 phylloquinones (referred to as A_1), and 3 Fe-S clusters as electron carriers, as well as 22–24 carotenoids (mainly β-carotene) as accessory pigments [4–6]. Whereas PSIs of plants and algae are monomeric, those of cyanobacteria are known to usually form a trimer with a small number of exceptions [7,8]. Most Chls bound to PSI serve as antennae, which efficiently transfer the absorbed light energy to the primary donor at the center of the complex. A classical postulate on Chls bound

Abbreviations: PSI, photosystem I; Chl, chlorophyll; SMS, single-molecule spectroscopy; ROS, reactive oxygen species; CS, conformational substates; *β*-DM, *n*-dodecyl *β*-D-maltoside; CCD, charge-coupled device; FWHM, full width at half maximum; ES, electrochromic shift; APC, atomic partial charge

* Corresponding author.
E-mail address: shibata@m.tohoku.ac.jp (Y. Shibata).
[1] Present address: School of Biology, Biomedical Science Research Complex, University of St Andrews, North Haugh, St Andrews, KY169ST, United Kingdom.
[2] Present address: Research Institute of Interdisciplinary Science, Okayama University, Tsushimanaka, Kita-ku, Okayama 700-8530, Japan

https://doi.org/10.1016/j.bbabio.2018.11.002
Received 12 June 2018; Received in revised form 21 August 2018; Accepted 4 November 2018
Available online 11 November 2018

to a photosystem is that their excitation energies form a gradient toward the primary-donor Chl for efficient light harvesting. The gradient is realized by fine tuning the environment of each Chl binding site to adjust its excited-state energy. Hereafter, we refer to the excited-state energy of a Chl molecule tuned by the protein environment as the "site energy" of the molecule.

Although the above postulate of the biased site-energy gradient is basically the case, it has long been known that there are several exceptions to this general rule. It is well-known that for PSIs isolated from many organisms, whereas most bound Chls have site-energies higher than that of the reaction-center pigment called P700, several Chls have considerably lower site energies than P700. They are responsible for the low-temperature emission band of PSI observed at around 710–760 nm depending on species [9–11]. In this article, we call this red-emitting state in PSI "red Chls". An early persistent-hole-burning study estimated the total absorption strength of red Chls to be equivalent to that of 9–11 Chl molecules for PSI isolated from a cyanobacterium *Thermosynechococcus* (*T.*) *elongatus* [12]. Hole-burning studies on PSIs in combination with the measurements of the Stark effect also revealed strong electron-vibration couplings of the red-Chl [13,14], suggesting their charge-transfer nature.

The red-Chl pools in PSIs are considered to contribute to expanding the absorption cross section of PSIs to the redder spectral region [15]. In addition, an increasing number of studies have suggested its protective role [10,16–18]. Under a situation where the usual photosynthetic electron transport is limited, chances to generate reactive oxygen species (ROS) increase due to repeated charge-recombination processes at the primary donor or undesirable electron donations to oxygen molecules. To reduce the chance of ROS generation, the oxidized form of the primary donor, $P700^+$, has been considered to serve as an efficient excitation-energy quencher. Since the red Chl has an appreciable spectral overlap with $P700^+$ having its broad absorption band at around 800 nm [19,20], it has been considered to function as an intermediating pigment that accumulates excitons from the major antenna Chls and directs it to $P700^+$. The strong electron-vibration coupling of the red Chl ensures its large Stokes shift, which is advantageous for enhancing the spectral overlap with the $P700^+$ absorption band. PSI of *Arthrospira platensis* shows an especially red-shifted emission at around 760 nm. This band is substantially quenched upon P700 pre-oxidation, giving clear evidence for the intermediating role of the red Chl [21,22]. Although the very larger red shift of the emission peak of *P. platensis* PSI is striking, it has been revealed that the nature of the Chl responsible for the red-shifted emission of this organism is similar to those in the other cyanobacterial PSI [22].

SMS on PSIs have revealed interesting properties of red-Chl pools and the energy-transfer dynamics within PSI [1,23–29]. The primary interest of earlier studies was mainly directed at revealing photo-physical properties of red Chls in PSI and actually confirmed the strong electron-phonon couplings of the red Chl characterized by a large Huang-Rhys factor [1,23,25]. In addition, these studies have opened a fruitful research field of conformation fluctuation dynamics of PSIs at cryogenic temperatures. The sharp zero-phonon line shows frequent peak-position jumps, reflecting the fluctuation in the surrounding environment of the observed pigment [1,28,29]. Based on the experiment of the isotope effect, the spectral hopping was attributed to the movement of a proton near the emitting pigment [1].

The observation of fluctuating fluorescence spectra of single PSIs can be associated with the concept of the ragged potential-energy landscape of a protein, which was originally proposed by Frauenfelder et al. [30,31] based on their pioneering works on the temperature-dependent X-ray diffraction of a protein crystal. It was proposed that because of the many conformational degrees of freedom in a protein molecule it has a huge number of metastable states with slightly different conformations of amino acid residues. These metastable states were conceptually named Conformational Substates (CS). The fluctuations of fluorescence spectra observed in the SMS study on PSIs and other photosynthetic complexes like LH2 [32] can be regarded as reflecting the hopping among CSs divided by small energetic barriers.

Although the first SMS study on PSI was conducted within a wide temperature range from 1.8 K to 236 K and clarified the rather high photostability of PSI even at high temperatures above 200 K [23], subsequent studies have been done mainly at cryogenic temperatures below 10 K. At such low temperatures, conformation dynamics are considered tightly limited to tiny movements such as those of protons [1]. For better understanding of the conformational dynamics released at higher temperatures, SMS studies of PSI at higher temperatures are needed. We can expect larger and more frequent fluctuations of fluorescence spectra of single PSIs at higher temperatures due to larger-scale conformational motions activated by the input of thermal energy. Recently, we have developed a novel cryogenic microscope system with a new configuration, in which the microscope objective lens is set inside the heat-insulating vacuum chamber [33]. Thanks to this configuration, the working distance could be drastically reduced, enabling the usage of a highly chromatic-aberration-corrected objective lens with a high numerical aperture of 0.9. In the present study, we use the developed system to conducted SMS on PSI trimers isolated from a cyanobacterium, *Synechocystis* sp. PCC 6803, at around the boiling temperature of liquid N_2. In this study, we found that pre-oxidation of P700 enhances the amplitude of fluorescence blinking. The different blinking amplitude can be attributed to the different redox state of the secondary acceptor phylloquinone (called A_1). We discuss possible mechanisms for the A_1-redox-state dependent blinking.

2. Materials and methods

2.1. Sample preparation

To isolate the PSI trimers, the cyanobacterium *Synechocystis* sp. PCC 6803 47-H strain, which has a six-histidine tag at the C-terminus of the CP47 subunit, was grown in BG11 medium under a photoautotrophic condition [34]. Thylakoid membranes were prepared in accordance with the method described previously [34]. Thylakoids suspended in a buffer (pH 6.0) containing 50 mM MES-NaOH, 5 mM $CaCl_2$, 10 mM $MgCl_2$, and 25% (w/v) glycerol (buffer A) were solubilized with 1% (w/v) *n*-dodecyl *β*-D-maltoside (*β*-DM) at a Chl concentration of 1.0 mg/mL by stirring for 10 min on ice. After centrifugation at 27000*g* for 15 min, the resultant supernatants were applied to a Ni^{2+} affinity column equilibrated with buffer A containing 0.04% *β*-DM (buffer B). PSI complexes were fractioned with buffer B containing 100 mM imidazole-HCl (pH 6.0) and 100 mM NaCl, whereas PSII core complexes were bound to the Ni column without elution. The PSI fraction was further applied to a TOYOPEARL DEAE-650 M column (Tosoh) equilibrated with a buffer (pH 7.5) containing 50 mM HEPES-NaOH, 5 mM $CaCl_2$, 10 mM $MgCl_2$, 50 mM NaCl, 0.03% *β*-DM, and 25% (w/v) glycerol (buffer C). After washing the column with buffer C until the eluent became colorless, PSI core complexes were eluted with buffer C containing 500 mM NaCl.

The PSI solution was divided into a small volume of tubes and stored in a freezer (−78 °C) until use. For an SMS experiment, a thawed stock of a PSI solution was diluted to a trimer concentration of 7 pM with a buffer, pH 7.5, 20 mM Tricine-HCl containing 25 mM $MgCl_2$, 0.02% (w/v) *β*-DM. We centrifuged the solution with a rotation speed equivalent to 14,000 g for 300 s at 4 °C just before the final dilution step to remove the aggregated complexes. 1-mM sodium ascorbate was added to the buffer to maintain P700 in its neutral form, while 1-mM potassium ferricyanide was added for the pre-oxidation of P700. We confirmed the difference spectrum of the P700 pre-oxidized minus pre-reduced conditions, characterized by a 700-nm bleach of P700 and a broad absorbance at around 800 nm due to $P700^+$ (data not shown). In the present study, we did not add any cryoprotectant like glycerol to the sample solution. The effect of addition of glycerol on the low-temperature emission properties of PSI of *T. elongatus* was studied by the

single-molecule spectroscopy by Hussels and Brecht [29]. They found an enhanced heterogeneity of the emission properties of single PSI when the addition of glycerol was omitted. The enhanced heterogeneity might be due to partial crystallization of water molecules surrounding the protein. On the other hand, the fluorescence spectra averaged over molecules were similar between samples with and without glycerol, indicating that omitting glycerol induced no severe damage to the protein structure. Thus, it remains an open question which condition, with or without cryoprotectant, better reflects the physiological characteristic of PSI.

The sample solution was introduced to a homemade copper sample holder as previously reported [33]. A few μL of the sample solution was put in a hole of a greased Teflon spacer on a quartz window with a thickness of 0.3 mm. The solution was then sealed with another glass window from the top and set in the sample holder. The holder was set in the vacuum chamber of the cryo-microscope and connected to the cold head of the cryostat (Microstat, Oxford Instruments, Eynsham). The sample temperature was monitored with a gold/iron-chromel thermocouple and cooled to 80 K by the flow of liquid N_2. The sample temperature reaches to 80 K typically within 30-min after the start of the liquid N_2 flow. We confirmed in the previous paper [33] that the positioning stability of the sample stage of the setup is sufficient for chasing the fluctuation in a single-molecule fluorescence spectrum for several minutes. Red-emitting fluorescent beads with a diameter of 200 nm (F8807, Molecular Probes) were dispersed in a poly-vinyl alcohol aqueous solution (1% w/w) and spin coated on a quartz window (0.3 mm thick and 10 mm in diameter) with a spin coater (1H-D3, Mikasa, Tokyo) at 500 rpm for 15 s and then 4000 rpm for 60 s. The coated quartz window was introduced to the cryo-microscope as described above.

2.2. Redox state of co-factors during the experiment

It has been established that, at low temperature, some fraction of PSIs repeat cycles of charge separation and recombination between the primary donor P700 and the primary and secondary acceptors A_0 and A_1 or the next acceptor F_x while another fraction irreversibly charge separated after excitation [35]. Schlodder et al. have clarified that below 150 K 45% of PSI repeat charge-separation-recombination cycles between P700 and phylloquinone, the secondary acceptor A_1 [35]. In the other fraction of PSI, slow reversible electron transfer to F_X (20%) and irreversible accumulations of $P700^+F_A^-$ and $P700^+F_B^-$ (35%) take place. The half lifetime of A_1^- in the former 45% fraction was estimated to be around 170 μs below 150 K [35,36]. The excitation rate k_{exc} is a product of the photon-flux and the absorption cross section given by $10^3 \cdot \ln(10)\varepsilon/N_A$, where ε is the molar-extinction coefficient in the unit of $M^{-1}\,cm^{-1}$. By using the value of ca. $10^4\,M^{-1}\,cm^{-1}$ for ε of Chl at 633 nm multiplied by ca. 90, the number of the Chl molecules per P700, the excitation rate k_{exc} of P700 can be roughly estimated to be $3.4 \times 10^8\,s^{-1}$ for the present 40-μW excitation focused to a spot with a diameter of 400 nm. Thus, unless we carefully use a very low excitation power as done by Schlodder et al. [11], in a P700 pre-reduced sample a state of $P700^+A_1^-$ is accumulated during the excitation. For a P700 pre-oxidized sample, on the other hand, A_1 remains neutral during the excitation because $P700^+$ serves as an effective excitation quencher rather than causes the charge-separation reaction.

2.3. Optical setup

The optical setup used in the present study is basically the same as that reported in the previous paper [33]. A He-Ne laser (1137P, JDS Uniphase, Milpitas) passed through a laser-line filter (NT65-753, Edmund Optics) was used as the excitation source. The laser beam was reflected by a dichroic mirror and focused on the sample with a vacuum-compatible objective lens (Plan Apo HR100× NA0.9, Mitutoyo, Kawasaki). The fluorescence was collected with the same objective lens, passed through the same dichroic mirror, and focused on the square entrance slit of the polychromator (MS2004i, SOL Instruments, Minsk). A liquid N_2-cooled charge-coupled device (CCD) camera (PyLoN:100BR eXcelon, Princeton Instruments, Trenton) was used as the detector.

2.4. Estimation of electrochromic shift

The electrochromic shifts (ES) of Chls bound in PSI induced by the negative charge on the phylloquinone were calculated based on the structure of PSI from PCC6803. We used either the values of the difference of atomic partial charges (APC) Δq of Chl-*a* between its electronic excited and ground states or the change in the permanent dipole moment $\Delta\vec{\mu}$ of Chl-*a* (dipole approximation). The values of Δq recently reported by Müh et al. [37] were used. Their estimation of Δq was based on the quantum chemical calculation of a single Chl-*a* isolated in vacuum based on the Hartree-Fock configuration interaction singles with the 6–31 g* basis set. In the calculation, the phytyl chain was replaced with a methyl group. The ES value of each Chl was calculated as electrostatic interaction energy between Δq of the Chl and the negative charge on the phylloquinone,

$$ES_{APC} = \frac{1}{\varepsilon_{eff}} \sum_{i,j} \frac{\Delta q_i \cdot q_j}{|\vec{r_i} - \vec{r_j}|}. \quad (1)$$

In the calculation, delocalization of the excited state was not taken into account. In Eq. (1), Δq_i and $\vec{r_i}$ are the difference of APC of the *i*-th atom of a Chl of interest and its coordinate, respectively. q_j and $\vec{r_j}$ are the negative charge on the *j*-th atom of phylloquinone and its coordinate, respectively. We assumed that the negative charges on the phylloquinone are equally distributed over atoms consisting its aromatic ring. We used a value of 1.5 for ε_{eff}, the effective dielectric constant of the protein matrix. The ES value based on the dipole approximation was calculated according to

$$ES_{DP} = \frac{1}{\varepsilon_{eff}} \sum_{j} \frac{\Delta\vec{\mu} \cdot (\vec{r}_{Mg} - \vec{r_j}) q_j}{|\vec{r}_{Mg} - \vec{r_j}|^3}. \quad (2)$$

Here, $\vec{r}_{Mg}$ is the coordinate of the central Mg atom of a Chl-*a* of interest. The value of $\Delta\vec{\mu}$ has been reported to have an amplitude of 0.5–1.0 D and be parallel to the vector from N_B to N_D nitrogen atoms [13,14,38,39]. In this study, we assumed a value of 0.7 D for the amplitude of $\Delta\vec{\mu}$ and its orientation parallel to the vector from N_B to N_D. This assignment is consistent with the estimation of $\Delta\vec{\mu}$ using the atomic partial charges Δq described above.

3. Results

3.1. Inhomogeneous distribution

First, we carried out measurements of fluorescence images of PSI trimer solutions at 80 K with stepwise dilutions from 700 pM to 70 pM, and finally to 7 pM. Typical results of such measurements are shown in Fig. S1 of the Supporting Information. Spatial distributions of fluorescence signals became sparse with decreasing concentrations to 70 pM. Finally, images containing isolated bright spots were obtained with a concentration of 7 pM. This observation is consistent with an estimation taking into account ca. 1.5-μm axial resolution of the current set-up that the 7-pM concentration corresponds to a situation where one will observe 0.6 PSI trimers per 10 μm × 10 μm square on average. Owing to the centrifugation of the sample solution just before use, it was very rare to find particles assigned to aggregated complexes emitting much more intense emission than the average. Thus, we consider that isolated fluorescent spots observed with 7-pM samples come from single PSI trimers.

Fig. 1 shows examples of fluorescence spectral changes of single PSI trimers during consecutive spectral measurements for 220 s.

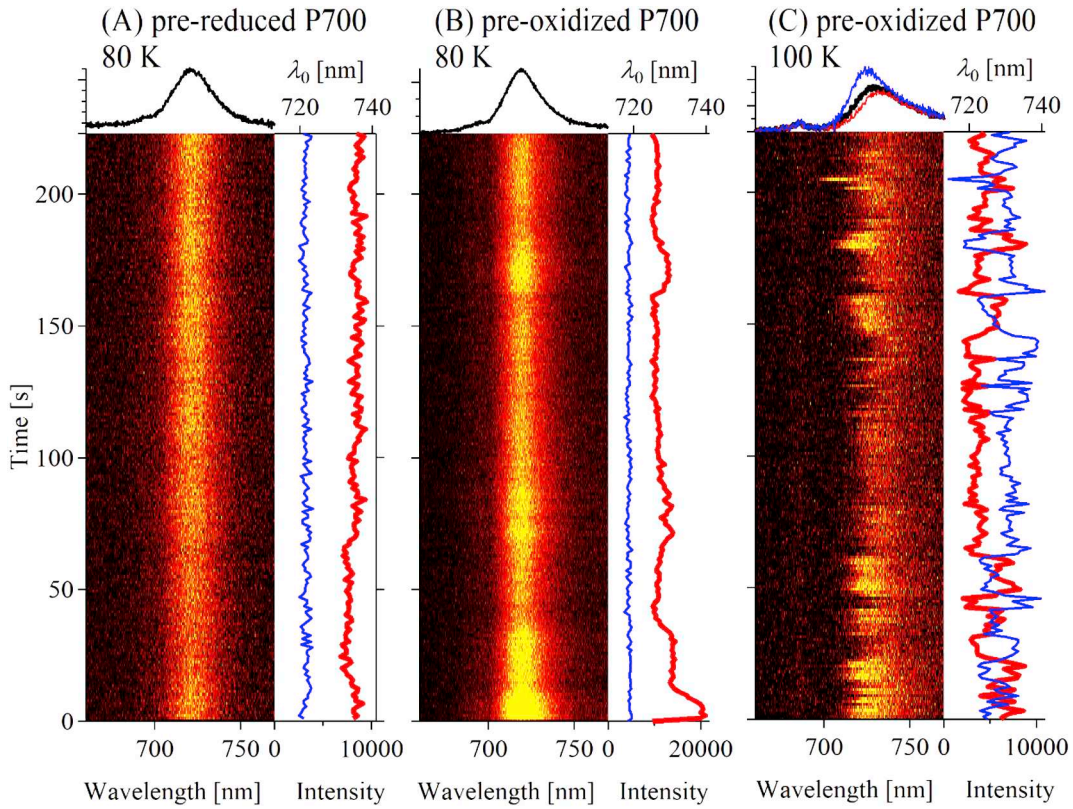

Fig. 1. Examples of time evolutions of fluorescence spectra of single PSI trimers containing pre-reduced P700 and observed at 80 K (A), containing pre-oxidized P700 and observed at 80 K (B) and at 100 K (C). The time sequence of 199 spectra with an accumulation time of 1 s and dead time of 0.12 s for each are displayed in the lower left panel. Red and blue lines in the right panels show the fluorescence-signal intensities integrated over a range of 710–740 nm (bottom axis) and the peak wavelength (top axis) estimated by the fitting (see text), respectively. The time-averaged fluorescence spectra over the whole 220-s observations are shown by black lines in the top panels. The blue and red spectra in the top panel of (C) show the fluorescence spectra averaged over the time regions showing blue-shifted and red-shifted emission spectra, respectively. (For interpretation of the references to color in this figure legend, the reader is referred to the web version of this article.)

Measurements were taken by pointing the focus spot of the excitation laser on a PSI molecule found in a pre-scanned image. Fig. 1A shows the result obtained for a single PSI trimer with neutral (pre-reduced) P700 by the addition of sodium ascorbate and measured at 80 K, while panels B and C show results for two individual molecules with pre-oxidized P700 by the addition of potassium ferricyanide and measured at 80 K and at 100 K, respectively. In the lower panel of Fig. 1, stacked 199 spectra, each taken with a 1-s accumulation and a dead time of 0.11 s, are displayed. Fluorescence signal intensities integrated over a 710 to 740-nm spectral range are plotted against the time (vertical axis) with the thick red lines in the panels on the right. One can see intermittent fluctuations of fluorescence intensity for the molecules displayed in panels B and C. This fluctuation of fluorescence intensity is called "blinking." In the case of the molecule displayed in panel C, frequent peak-position jumps, called "spectral diffusion," were observed in addition to the concomitant blinking. The spectral diffusion observed for the molecule displayed in Fig. 1C was reproduced by 4 repeated measurements. Although the fluorescence intensity of the molecule shown in Fig. 1A seems to be stable, a detailed analysis outlined below revealed that this molecule also showed an intensity fluctuation of the emission (blinking) beyond the detection limit of the current experimental system, which was estimated by the data of fluorescent beads. The black curves in the upper panel show fluorescence spectra averaged over the 199 spectra.

To clarify the distribution of emission peak position and quantify the degree of spectral diffusion during consecutive measurements, we obtained the time dependence of the peak wavelength of the spectrum by fitting it to the sum of two skewed Gaussian functions [40,41] expressed as

$$F(\nu) = \sum_{i=1,2} F_i \exp\left(-\ln 2 \cdot \left[\frac{1}{b_i}\ln\left(1+\frac{2b_i(\nu-\nu_{0,i})}{\Delta\nu_i}\right)\right]^2\right) \quad \ldots 1+\frac{2b_i(\nu-\nu_{0,i})}{\Delta\nu_i} > 0$$
$$= \quad 0 \quad \ldots 1+\frac{2b_i(\nu-\nu_{0,i})}{\Delta\nu_i} \le 0 \qquad (3)$$

The fitting was conducted to spectra plotted against wavenumber ν. Here, F_i, $\nu_{0,\ i}$, and $\Delta\nu_i$ are the amplitude, peak wavenumber, and bandwidth of i-th component, respectively. The first and second components in Eq. (3) are assigned to the emission bands around 720 nm (the red Chl band) and those around 690 nm (the bulk Chl band), respectively. For some molecules, we observed a weak sub-band at around 690 nm, as shown in Fig. 1B and C. To fit the data of these molecules, we needed the second component. b_i is the asymmetry parameter of i-th component. A negative/positive b_i gives a gentler slope on the lower/higher wavenumber side of the band. At the limit of $b_i = 0$, the curve converges to a Gaussian function. As shown in Fig. S2 in the Supporting Information, all measured spectra could be well reproduced with this model curve. The blue lines in the right panels of Fig. 1 show the estimated peak wavelengths λ_0 of the fluorescence spectra at the given time, which were calculated as the reciprocal of ν_0. The right panel in Fig. 1C clearly visualizes the spectral diffusion as well as the simultaneous blinking. It should be noted here that the data shown in Fig. 1C were obtained by an experiment carried out at 100 K which is higher than those in Fig. 1A and B. As shown below in Fig. 2, in the present study it was very rare to find molecules showing the spectral diffusion typically shown in Fig. 1C.

The bars in Fig. 2 show the histograms of the peak wavelength, λ_0, averaged over the 220-s time sequence estimated for each single

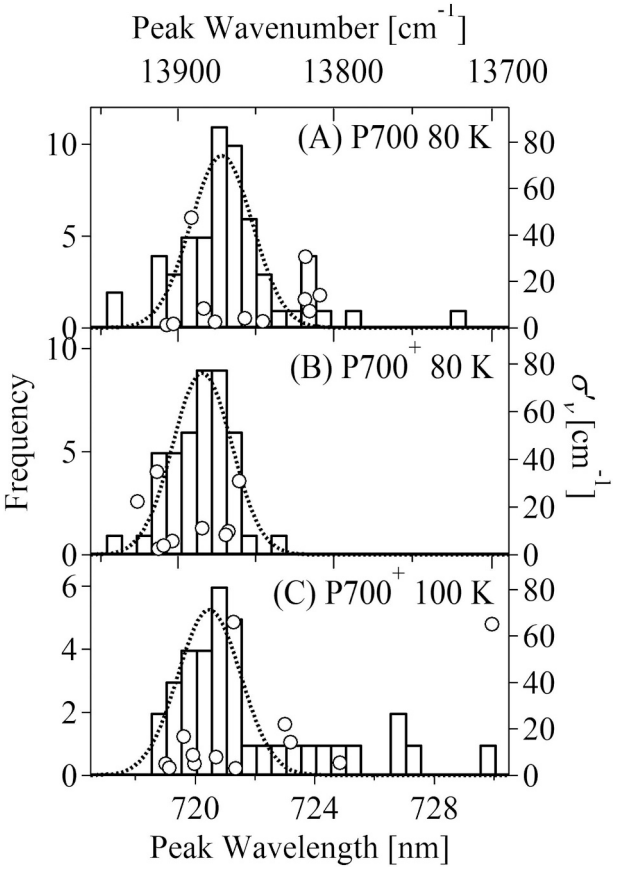

Fig. 2. Bars show histograms of the averaged peak wavelengths (left axes) for single PSIs with reduced P700 measured at 80 K (A), those with oxidized P700 measured at 80 K (B), and at 100 K (C). The histograms in (A), (B), and (C) were calculated with data of 58, 44, and 36 molecules, respectively. Dotted lines are the fitting curves of the histograms to Gaussian functions. Open circles indicate the standard deviations of the peak wavenumbers during the 220-s time evolutions (right axes). Only data points that are significantly larger than the confidence interval (see text) of the fitting are plotted.

molecule. Thus, they are the histograms for N spectra, with N being the number of molecules observed under the given conditions. The numbers of measured molecules N were 58, 44, and 36 for the data in panels (A), (B), and (C), respectively. It is important to point out here that the inhomogeneous distribution generally depends on the time scale or time resolution of the measurement used. The histograms shown in Fig. 2 are regarded as apparent inhomogeneous distributions of the emitting Chl with the time resolution of 220 s at given conditions. Although we found several molecules showing peak shifts to 730 nm (especially in Fig. 1C), the majority of molecules had emission peaks at around 720 nm. The population of such exceptional molecules with the 730-nm emission peaks is reflected in the tail of histograms extending to 730 nm (Fig. 2). We fitted the obtained histograms to Gaussian functions (dotted lines), and summarized the parameters obtained by the fitting in Table 1. Here, FWHM listed in the table is the estimate of the inhomogeneous width with the time resolution of 220 s. The peak position and width of the histogram did not show noticeable temperature dependence. On the other hand, the histogram of PSI with pre-oxidized P700 observed at 100 K expanded to the side of the longer wavelength, giving a small second peak at around 726 nm. This may suggest the emergence of an additional state, giving rise to a fluorescence band at around 726 nm.

We also calculated the standard deviation of the peak wavenumber (σ_{ν_0}) for each molecule,

Table 1
The peak wavelength (WL) and width of the histogram of averaged peak position of the single PSI spectra.

	80 K neutral P700	80 K oxidized P700	100 K oxidized P700
Peak WL [nm]	720.9 ± 0.2	720.2 ± 0.1	720.5 ± 0.2
FWHM [cm^{-1}]	47.0 ± 9.3	44.8 ± 5.8	47.7 ± 10.5

$$\sigma_{\nu_0} = \sqrt{\frac{1}{199}\sum_{j=1}^{199}[\nu_{0j} - \langle\nu_0\rangle]^2}\,, \tag{4}$$

where ν_{0j} is the peak wavenumber of the j-th spectrum in the 220-s chase, and $\langle X\rangle$ is the average of a quantity X over the 220-s chase. We thought this value could be regarded as a rough measure of the spectral diffusion of the molecule. However, since the confidence interval of the estimated ν_0 by fitting depends upon the signal intensity for each molecule, the σ_{ν_0} values cannot be a practical measure of the spectral diffusion. Data for a molecule with a low signal intensity results in a large fluctuation in ν_0 during the 220-s measurement and in a large value of σ_{ν_0} even if spectral diffusion does not actually occur. The confidence interval of the ν_0 value is proportional to the standard deviation $\Delta\nu_0$ estimated by the fitting iteration. When the estimated $\Delta\nu_0$ value is larger, the estimated value of ν_0 is less reliable. Thus, we corrected the value of σ_{ν_0} using the averaged value of $\Delta\nu_0$ for the molecule.

$$\sigma'_{\nu_0} = \sqrt{{\sigma_{\nu_0}}^2 - \langle\langle\Delta\nu_0\rangle\rangle^2}\,. \tag{5}$$

Here, $\langle\langle\Delta\nu_0\rangle\rangle$ is the weighted average of the standard deviation $\Delta\nu_0$ calculated according to an equation with a weighting factor of $1/{\Delta\nu_{0j}}^2$,

$$\langle\langle\Delta\nu_0\rangle\rangle = \sqrt{\sum_{j=1}^{199}\frac{1}{{\Delta\nu_{0j}}^2}{\Delta\nu_{0j}}^2 \Big/ \sum_{j=1}^{199}\frac{1}{{\Delta\nu_{0j}}^2}} = \sqrt{\frac{1}{\langle 1/{\Delta\nu_0}^2\rangle}}\,. \tag{6}$$

Among 199 spectra during the 220-s chase, some may have very low signal since the molecule is in the dark state. Fitting of such a noisy spectrum results in a very large $\Delta\nu_0$ value. In Eq. (6), we introduced the weighting factor of $1/{\Delta\nu_{0j}}^2$ to suppress the contributions from such erroneously large $\Delta\nu_0$ values. We picked up σ'_{ν_0} given by real numbers (${\sigma_{\nu_0}}^2$ is larger than $\langle\langle\Delta\nu_0\rangle\rangle^2$ in Eq. (5)) as rough measures of the spectral diffusion of the molecule. Open circles in Fig. 2 are the obtained σ'_{ν_0} values (right axis) for single PSI trimers. As pointed out above, large σ'_{ν_0} values beyond 40 cm^{-1} were observed only for a limited number of molecules. The majority of molecules gave σ'_{ν_0} values of less than 20 cm^{-1} and showed no clear spectral diffusion in this case. σ'_{ν_0} values beyond 60 cm^{-1} were observed only for two molecules with P700 pre-oxidized and observed at 100 K.

3.2. Blinking properties

To quantify the degree of blinking of individual PSI trimers, we next calculated the standard-deviation values (σ_I) of the fluorescence signal integrated over a wavelength range from 710 to 740 nm during the 220-s measurement for each single PSI. As a measure of the blinking, here we introduce a parameter, $\sigma_I/\langle I\rangle$, which is termed the coefficient of variation, defined as σ_I divided by $\langle I\rangle$, the average of the signal intensity during each 220-s measurement. The dots in Fig. 3 show $\sigma_I/\langle I\rangle$ values plotted against $\langle I\rangle$. To confirm that the observed blinking is not due to the mechanical instability of our homemade cryogenic microscope system, we conducted the same measurements for fluorescent beads as a control showing no blinking. The emission peak of the beads is at around 685 nm (Fig. S3 inset). We did the same 220-s chase of the emission intensity for 4 independent fluorescent beads as we did for the single PSIs. To make the signal intensity similar to that observed for the SMS measurements of PSI, we used low excitation powers ranging from 20 nW to 320 nW to measure the fluorescent beads. We obtained very

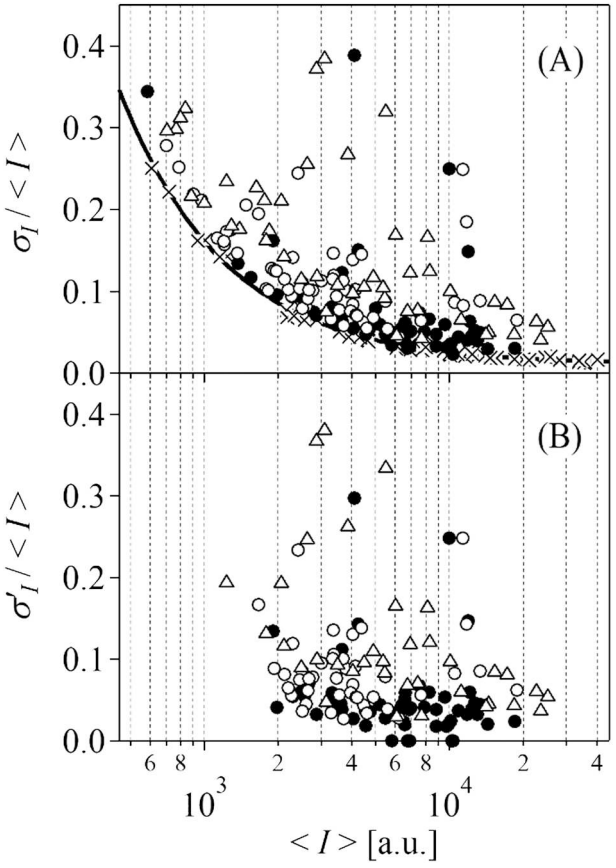

Fig. 3. (A) $\sigma_I/\langle I\rangle$ of fluorescence intensities over 220-s time sequences are plotted against the average $\langle I\rangle$. (B) The corrected standard deviation, σ'_I, divided by the averages, $\langle I\rangle$, is plotted against the average, $\langle I\rangle$. The σ'_I values were obtained by subtracting the contributions from the dark counts and read-out noise of the CCD camera, the photon shot-noise, and the mechanical instability of the system (see text for details). Closed circles, open circles, and open triangles indicate data points for PSI with pre-reduced P700 at 80 K, with pre-oxidized P700 at 80 K, and with pre-oxidized P700 at 100 K, respectively. Crosses in (A) are data points for the fluorescent beads. The solid line is the theoretical curve given by Eq. (7). Data points with averaged fluorescence intensities comparable to or below the standard deviation of the dark counts are rejected in panel B.

stable time sequences of the fluorescence intensity for the beads, confirming the absence of blinking (data not shown).

The data points indicated by crosses in Fig. 3A were obtained for the fluorescent beads, whereas those indicated by closed circles, open circles, and open triangles were obtained for the measurements of individual PSIs with neutral P700 at 80 K and those with pre-oxidized P700 at 80 K and at 100 K, respectively. The $\sigma_I/\langle I\rangle$ values for the fluorescent beads increased with decreasing average signal intensity, reflecting a degraded S/N ratio due to reduced signal intensity. It should be noted that the $\sigma_I/\langle I\rangle$ values of many single PSI trimers are significantly larger than those of fluorescent beads, suggesting that the observed blinking is not an artifact.

The solid line in Fig. 3A is a theoretical curve calculated based on an argument given in the Supporting Information. Here, we consider that the fluctuation of the fluorescence signal of the fluorescent beads comes from three contributions: (1) the dark counts and read-out noise of the detector, (2) the photon shot-noise, and (3) the mechanical instability of the instrument. Contribution (1) is determined by the performance of the CCD camera and does not depend on the signal intensity. The second component, the photon-shot noise, is known to obey Poisson statistics, characterized by the variance of the signal intensity linearly depending on the averaged signal intensity. The third contribution, mechanical fluctuation, will cause a slight wobbling of the focusing spot of the laser with respect to the position of the molecule observed. This results in the standard deviation of the signal-intensity fluctuation linearly depending on the signal intensity. In other words, the third contribution results in variance with a quadratic dependence on the signal intensity. It should be noted that the values of all data points in Fig. 3A were calculated using spectral data integrated over the same wavelength range from 710 to 740 nm to have the same dark-count and read-out noise contributions. The theoretical curve in Fig. 3A is obtained by assuming that the three contributions discussed above are not correlated with each other. Fig. S3 shows the result of the fitting of the coefficient of variance of the bead fluorescence based on the theoretical consideration outlined above and in the Supporting Information. The parameter values estimated by the fitting are listed in Table 2. In Fig. S3A, contributions from (1), (2) and (3) are indicated by a thin solid line, dotted line, and dashed line, respectively. The corresponding expression for the $\langle I\rangle$-dependence of $\sigma_I/\langle I\rangle$ plotted in Fig. 3A is given by,

Table 2
Estimated parameters from the fitting of the Variance/Average vs. the Average plot of the fluorescent beads.

A	B	C
24,000 ± 840	2.85 ± 0.52	$(1.01 \pm 0.10) \times 10^{-4}$

$$\frac{\sigma_I}{\langle I\rangle} = \frac{\sqrt{A + B\langle I\rangle + C\langle I\rangle^2}}{\langle I\rangle}. \tag{7}$$

The theoretical curve in Fig. 3A was calculated according to Eq. (7) using the parameters listed in Table 2. The curve gives the instrumental lower limit of detection of blinking in the present measurement.

Using the obtained instrumental curve in Fig. 3A, we can obtain corrected standard deviation values of individual PSI trimers, σ'_I, for which the fluctuation in the fluorescence signal inherent to the instrument was subtracted according to the following formula,

$$\sigma'_I = \sqrt{\sigma_{I,\mathrm{obs}}{}^2 - \sigma_{\mathrm{Instr}}{}^2} = \sqrt{\sigma_{I,\ \mathrm{obs}}{}^2 - (A + B\langle I\rangle + C\langle I\rangle^2)}, \tag{8}$$

where $\sigma_{I,\ \mathrm{obs}}$ is the uncorrected standard deviation of the fluorescence intensity of each individual PSI. Fig. 3B shows the corrected $\sigma'_I/\langle I\rangle$ values plotted against the averaged signal intensity $\langle I\rangle$.

To estimate the time scale of the observed blinking, we next calculated the autocorrelation functions, $C(\tau)$, of the fluorescence intensity time traces. $C(\tau)$ was calculated according to the following equation,

$$C(\tau_i) = \sum_{j=1}^{199-i} I_j \bullet I_{j+i}, \tag{9}$$

where I_j is the signal intensity of j-th time point. The instantaneous decay of $C(\tau_i)$ from the first to the second point is mainly due to the white-noise component coming from the instrument that is not of interest. Instantaneous decay was also seen for the $C(\tau_i)$ of fluorescent bead data. To zoom in on the slow protein-dynamics-induced part of the time variation in $C(\tau)$, we normalized the autocorrelation function so that its values at the second point, $C(\tau_2)$, achieve unity. Each red curve in Fig. 4 is, thus, calculated autocorrelation function for each observed individual PSI trimer. Autocorrelation function for all the measured molecules are shown in Fig. 4. Temporal changes in $C(\tau)$ are very small for PSI containing neutral P700 at 80 K, as shown in panel A. There is one trace with an exceptionally large temporal change, which was obtained for a molecule showing irreversible bleaching during the time trace measurement. Fig. 4B shows the $C(\tau)$ for PSI with pre-oxidized P700 at 80 K. It is clear that the pre-oxidation of P700 resulted in an increase of the fraction of molecules with larger temporal variation in $C(\tau)$. This tendency was further enhanced when the temperature was raised to 100 K, as shown in Fig. 4C, where the $C(\tau)$ of more fractions of molecules decreased to approximately 0.8. To estimate the time scale of

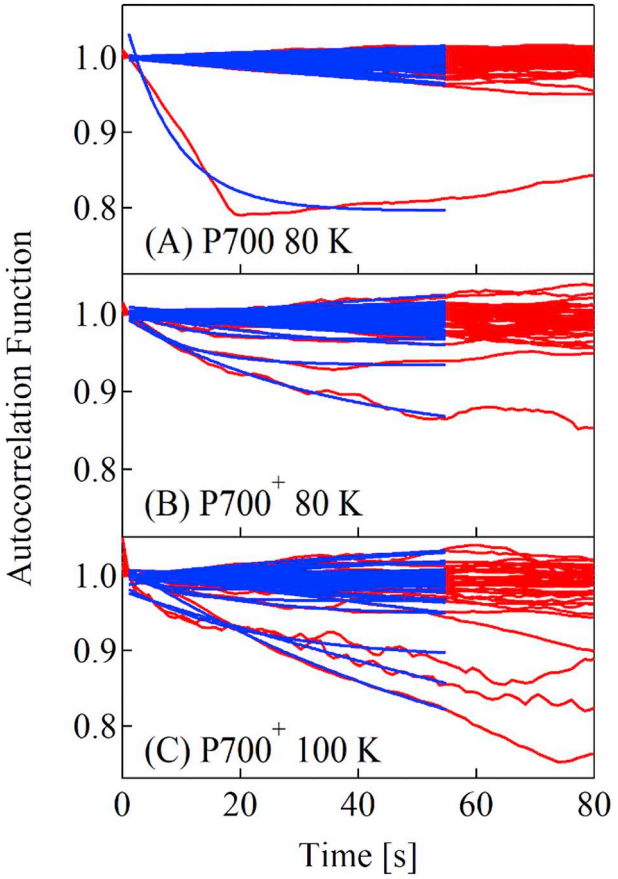

Fig. 4. Autocorrelation function (red curves) of the fluorescence intensity traces of single PSI with reduced P700 measured at 80 K (A), those with oxidized P700 measured at 80 K (B) and at 100 K (C). Blue lines show the fitting curves to single-exponential decay or rise curves. (For interpretation of the references to color in this figure legend, the reader is referred to the web version of this article.)

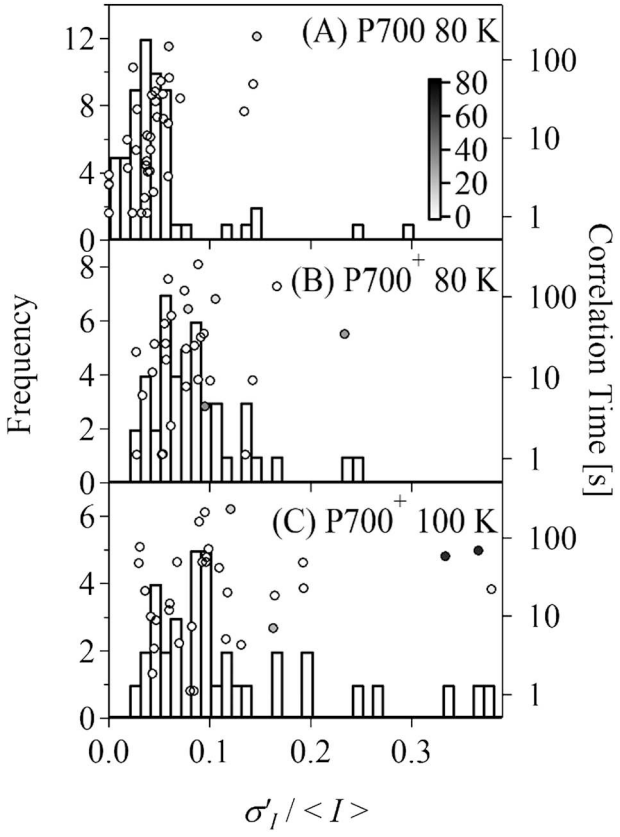

Fig. 5. Histograms of the corrected standard deviation, σ'_I, divided by the averages $\langle I \rangle$ (left axis) for single PSIs with reduced P700 measured at 80 K (A), those with oxidized P700 measured at 80 K (B), and at 100 K (C). Correlation times estimated by the fitting of the autocorrelation functions in Fig. 4 are plotted against $\sigma'_I/\langle I \rangle$ (circles, right axis). The density of the circles expresses the standard deviations of the peak wavenumber, σ'_{ν_0}, shown in Fig. 2. The scale of the density is shown by the color scale (unit in cm^{-1}).

the fluctuation, we fitted the autocorrelation functions in Fig. 4 to single exponentially decaying or rising curves as shown by blue lines. We conducted this fitting within a time sequence of the $C(\tau)$ ranging from 1 s to 55 s. The time constant obtained by the fitting is regarded as a rough measure of the correlation time. Correlation times for some molecules were estimated to be longer than the observation time of 220 s, reflecting the existence of slow dynamics for these molecules. We found that molecules showing large amplitudes of blinking tended to have correlation times of around several tens of seconds.

Fig. 5 compares histograms of the $\sigma'_I/\langle I \rangle$ values between PSIs containing neutral P700 at 80 K (A) and pre-oxidized P700 at 80 K (B) and 100 K (C). It is clear that the distribution of the $\sigma'_I/\langle I \rangle$ values was expanded to the right upon P700 pre-oxidation and the temperature rise to 100 K. Thus, as indicated in Figs. 3 and 4, the pre-oxidation of P700 increases the fraction of molecules with larger blinking. Fig. 5 also shows the correlation times estimated by the fitting of $C(\tau)$ to a single-exponential function. Molecules with large $\sigma'_I/\langle I \rangle$ values have correlation times ranging from 10 s to 100 s. We also display in Fig. 5 σ'_{ν_0}, the corrected standard deviation of the peak wavenumber given by Eq. (5) as a measure of the spectral diffusion. In Fig. 5, the darkness of the closed circles corresponds to the σ'_{ν_0} value shown in Fig. 2. Fig. 5 shows that a molecule with intense blinking tends to exhibit a large spectral diffusion.

3.3. Excitation-power dependence of blinking

Finally, we investigated the excitation-power dependence of the blinking of individual PSI trimers to clarify whether the observed blinking is light induced. If the excited state of Chl is involved in the induction of blinking, the degree of blinking depends on the excitation power and vice versa. We measured the same 220-s time sequence of single PSI spectra with 4 different excitation powers, 10, 20, 40, and 80 μW. By taking into account the laser spot size of ca. 400 nm in diameter, these excitation powers were estimated to correspond to 8.0, 16, 32, and 64 kW/cm^2, respectively. Fig. 6 panels A and B respectively show the excitation-power dependences of $\sigma'_I/\langle I \rangle$ and $\langle I \rangle$ obtained from the 199 consecutive spectral measurements for 5 individual PSI trimers. The averaged signal intensity $\langle I \rangle$ shown in Fig. 6B showed almost linear dependence on the excitation power up to 32 kW/cm^2. On the other hand, the plot in Fig. 6B showed signs of saturation at higher excitation powers. As discussed later, the maximum excitation power of 64 kW/cm^2 used here is predicted to cause the onset of singlet-singlet annihilation. Nonetheless, $\sigma'_I/\langle I \rangle$ averaged over the 5 molecules in Fig. 6A showed no considerable dependence on the excitation power. This result suggests that the observed blinking is induced mainly by a mechanism independent of light-irradiation.

4. Discussion

4.1. Site-energy fluctuation of C714

Although we found several molecules that showed frequent spectral diffusion (Fig. 1C), in the present experiment, the majority of molecules showed fluorescence-intensity jumps without considerable spectral

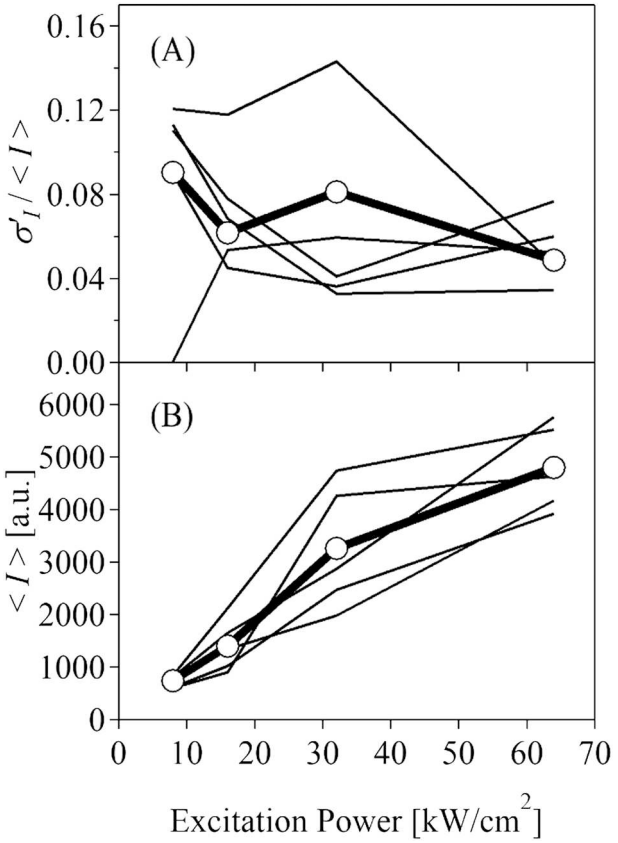

Fig. 6. The excitation power dependences of $\sigma'_I/\langle I\rangle$ (A) and the averaged fluorescence signal intensity $\langle I\rangle$ (B). Thin lines show data for 5 individual PSI molecules with reduced P700, and open circles connected by thick solid lines are averaged data for the 5 molecules.

diffusion. The spectral diffusion of PSI has been clarified as being so fast that it is hard to be resolved by a practical time resolution of SMS even at cryogenic temperature [1,27]. Random spectral shifts could be more readily accessible only when a deuterated buffer was used. This observation clearly indicated the involvement of the dynamic motions of exchangeable protons in the vicinity of the emitting Chls in the observed spectral diffusion. It should be noted here that the boundary between homogeneous and inhomogeneous broadenings depends on the time resolution of the measurement. In the present experimental condition, single PSIs showed broad fluorescence spectra governed by fast spectral diffusions that are not accessible by the present time resolution. The FWHM (full width at half maximum) of the spectra taken with the 1-s accumulation time was estimated to be around 400 cm^{-1}. This large bandwidth of the single PSI emission spectra is regarded as apparent homogeneous widths at 80–100 K with a given time resolution of 1 s.

The histogram of the peak wavelengths of single PSI emission spectra (Fig. 2 dotted lines) serves as an apparent inhomogeneous distribution at 80–100 K. Based on the hole-burning investigations [13,42], it has been established that there are two red Chl pools, called C706 and C714 after their absorbing wavelengths, for PSI trimers isolated from PCC 6803. The peaks of the histogram in Fig. 2 at around 720 nm can be assigned to C714. The early studies cited above revealed a large inhomogeneous broadening of ca. 300 cm^{-1} for the C714 pool of PCC 6803 PSI [42] and ca. 250 cm^{-1} for the C719 pool of *T. elongates* PSI [14]. These values are much larger than those typically reported for other photosynthetic proteins [43,44], probably due to the strong exciton-phonon couplings of these emitting states. A previous theoretical work also employed rather large values of 200–300 cm^{-1} for the inhomogeneous broadening of Chls in PSI [45]. By comparison, the distributions shown in Fig. 2 have a quite small FWHM of ca. 47 cm^{-1}, as summarized in Table 1. On the other hand, Riley et al. reported on an SMS study on PSI from PCC 6803 at 10 K [25]. The distribution of the fluorescence peak wavelength they obtained is sharp and similar to what we obtained in the present study.

If we take into account the concept of a protein's hierarchical energy landscape [30,31], a rising temperature is expected to allow the activations of larger conformational motions requiring interconversions between conformational substates divided by higher energy barriers. The apparent inhomogeneous broadening of 47 cm^{-1} in the 80–100 K region is much smaller than the value of 300 cm^{-1} estimated by experiments done at lower temperatures below 2 K, while it is similar to that estimated by the SMS study done at 10 K [25]. This indicates that conformational dynamics activated below 10 K already causes a dominant contribution to the site-energy shifts of C714. This means that tiny localized conformation changes around a pigment are sufficient to induce a major part of the total inhomogeneous broadening observed at cryogenic temperatures. Only a minor site-energy shift originates from a larger-scale conformation change released by increasing temperatures. Several studies have pointed out that the spectral diffusion of photosynthetic proteins observed by an SMS study at cryogenic temperatures is at least partially light-induced [32]. Thus, fast spectral diffusion, even at 10 K, might be due to the irradiation of a strong excitation laser enhancing light-dependent spectral diffusion.

We must be careful to generalize the above argument to other Chls bound to PSI. It might be applicable to C714, which is responsible for the red fluorescence emission of PSI but not to others. A theoretical study by Adolphs et al. analyzed the electrostatic interactions between Chls and the surrounding amino acid residues giving rise to site-energy shifts [45]. The study clarified that for many Chls bound to PSI, their site energies were determined by interactions with many amino acid residues. Some amino acids lower the site energy of the Chl, whereas the others lift it up. It is expected that conformation fluctuations of these amino acids are not correlated with each other. As a result, the site-energy fluctuation induced by fluctuations of many amino acids becomes small due to averaging out. Thus, for these Chls the site energies are stabilized by interactions with many amino acid residues. On the other hand, the analysis revealed another type of Chls for which the site energies are determined exclusively by interaction with a single amino acid. For the latter type of Chl, we expect a more labile site energy susceptible to the fluctuation in the amino acid residue responsible for the site-energy shift of the pigment. The different modes of pigment-protein interactions described above may result in different temperature dependencies of apparent homogeneous and inhomogeneous broadening of individual Chls.

Although it was rare, we found a few examples of spectral jumps of single PSI fluorescence spectra between ca. 720 nm and 730 nm as shown in Fig. 1C. There is a minor peak at around 726 nm in the histogram in Fig. 2C. Thus, there seem to be minor conformations in the amino acid residues surrounding C714 to induce an emission peak at around 726 nm. The populations of such conformations are very limited at 80–100 K. The fact that spectral diffusion was observed only at 100 K implies that raising the temperature enhances the population of conformations giving rise to the 726-nm emission. To confirm this, we need to do experiments at even higher temperatures. It is not clear whether the observed spectral jumps are due to the site-energy fluctuation of C714 or intermittent conversions of the terminal emitter from C714 emitting at 720 nm to that emitting at 726 nm. Because each single PSI trimer contains three sets of C714, it is likely that each of the three C714s has a different emission peak wavelength. In this case, the blinking of one or two of the three results in spectral diffusions as observed. This interpretation was also given to the spectral diffusion observed at cryogenic temperatures [28]. Averaged spectra in the blue-shifted and red-shifted time periods in the top panel of Fig. 1C suggest that blue shifts occur without any appreciable decreases in the red-spectral region. This suggests that the blinking of C714 with the

emission peak at 720 nm is a plausible explanation for the observed spectral diffusion.

4.2. Variable energy-transfer pathway

Intensity changes without appreciable spectral shifts were the most commonly observed mode of fluorescence fluctuation in the present study. We regard the observed fluorescence-intensity jumps to be caused by the redistribution of excitation energy between C714 and $P700^+$ known to function as an efficient fluorescence quencher [11,46,47]. Since we confirmed that the difference spectrum between the P700 neutral and oxidized conditions is mainly assigned to the redox reaction of P700, we can exclude the possibility that a cation of an antenna Chl other than P700 functions as a fluorescence quencher. Actually, the fluorescence quenching activity of $P700^+$ has been known to have a photoprotective role [10,17]. On the other hand, it has been known that β-carotenes bound to PSI also have a photoprotective role. However, their photoprotective activity is mainly based on the quenching of the Chl triplet state, not on their fluorescence quenching ability [48]. Thus, here we exclusively consider $P700^+$ as the fluorescence quencher in PSI.

We consider that the observed blinking is induced by fluctuation in the energy-transfer pathway due to the conformational dynamics of the protein. The antenna Chls in PSI are densely packed in the outer region of the elliptical structure of the PSI monomer. They are connected to each other through the very fast sub-ps energy-transfer process and form an energy-transfer network. On the other hand, there is a space between the antenna Chls and the redox-active Chls located at the central part of the complex that keeps the two groups of pigments away from each other to prevent unwanted electron-transfer reactions in the antenna pigments. The particular Chls, Chl-A840 and B839 (co-factor numbering is according to pdb 5OY0) near the phylloquinone, are called linker or bridging pigments, since their binding sites are in the interface between the antenna and redox-active pigment pools (see Fig. 7). We can expect that a large fluctuation in the site energy of Chl near the bridging Chls impacts the overall energy-transfer dynamics.

We consider that a Chl whose site energy is determined by interaction with a small number of amino-acid residues will show a large site-energy fluctuation and have a large impact on the overall energy-transfer pathway. As discussed above, the study by Adolphs et al. clarified 14 exceptional Chls for each of which the interaction with a neighboring single amino-acid residue has a dominant contribution to determine its site energy. Since these Chls are expected to experience heavily fluctuating electric field induced by the conformational dynamics of the single amino-acid residue, they are potential candidates to cause temporally variable energy-transfer pathway. The calculation by Adolphs et al. was done based on the crystal structure of *T. elongatus* PSI. It is found that the amino acids having dominant contributions to the site-energies of the 14 Chls are conserved in the recently resolved structure of *Synechocystis* PSI [6]. The present study revealed that the blinking was enhanced upon the pre-oxidation of P700 (Fig. 5). The different blinking properties between the P700 pre-reduced and pre-oxidized samples might be due to the different redox states of the secondary acceptor, phylloquinone (A_1). For the P700 pre-oxidized sample, A_1 remains in its neutral form, whereas for the P700 pre-reduced sample it will be in the anionic form on average. Thus, the existence or non-existence of a negative charge on phylloquinone is considered to cause the different properties of blinking. In the present study, we observed more salient blinking for the P700 pre-oxidized PSI in which phylloquinone remains in its neutral form.

We estimated the electrochromic shifts (ESs) of every Chls bound to PSI as listed in Table S1 in supporting information. From the calculation, we found two Chl-*a*'s, Chl-A802 (the primary acceptor called A_0) and Chl-A839, for which calculations based on both APC and the point dipole consistently gave large ESs (see Fig. 7 for the pigment arrangement). The estimated ES values for A_0 and Chl-A839 are negative and positive, respectively. As shown in Fig. 7, Chl-A839 is located near the bridging Chl, and therefore expected to have a large impact on the energy flow to the redox active pigment group. Further, we found that a Chl (A838) adjacent to Chl-A839 was one of the 14 Chls predicted to have a site energy determined by the interaction with a single amino-acid residue. The positive charge on a nearby arginine residue ArgF84 (ArgF82 in *T. elongatus* PSI) was predicted to have a dominant contribution to the -135-cm^{-1} stabilization of the site-energy of this pigment. Chl-A838 and A839 interact with each other by a strong exciton coupling. According to the arguments above, we speculate that a pair of Chls, Chl-A838 and A839, is involved in the enhanced blinking upon the P700 pre-oxidation.

Here we propose a possible scenario that the fluctuation of the site energy of Chl-A838 due to the conformation fluctuation in ArgF84 disturbs the ratio of exciton funneled to either $P700^+$ or C714, resulting in the observed blinking. The pre-oxidation of P700 maintains the phylloquinone in its neutral form, which results in a large negative shift of the site energy of Chl-A839 from the value in the P700 pre-reduced sample. Since Chl-A839 is strongly coupled to Chl-A838, the large ES of Chl-A839 may affect the exciton flow involving Chl-A838 and cause the P700 redox dependence of the blinking property. The proposed scenario is schematically depicted in the upper part of Fig. 7 and summarized as follows. In this model, we assume that in the phylloquinone reduced state (top-left panel of Fig. 7) the site energy of Chl-A839 is higher than that of Chl-A838 irrespective of the conformation of ArgF84 and unfavorable to accept the excitation energy from Chl-A838. On the other hand, in the phylloquinone neutral state (top-right panel of Fig. 7) the excited state of Chl-A839 is lowered ca. $40\ \text{cm}^{-1}$ (2 nm) and then the energy-transfer pathway varies according to the conformation of ArgF84. Thus, in this model the site-energy-fluctuation of Chl-A838 is the direct origin of the variation in energy-transfer pathway, and a neutral phylloquinone lowers the site energy of Chl-A839 and enhances the effect of Chl-A838. We observed a modest effect of the P700 pre-oxidation on the blinking, probably because only 45%, not 100%, of PSI accumulates $P^+A_1^-$ state [35]. The study by Adolphs et al. suggested an asymmetric site-energy distribution within PSI. Chl-A838-A839 pair is involved in a pigment domain with low exciton states, implying the accumulation of exciton in this pigment. This provides additional support for the above scenario, assuming a key role of the Chl pair on the fluorescence blinking.

4.3. Dependences of the blinking on excitation power

The excitation rate k_{exc} of $3.4 \times 10^8\ \text{s}^{-1}$ estimated for the current experimental condition suggests that one of the Chls bound to an individual PSI is excited every 2.9 ns ($=k_{exc}^{-1}$). Considering the ca. 1.5-ns lifetime of the excited state of the red Chls in PSI [46,47], we cannot ignore the onset of singlet-singlet annihilation. Nonetheless, we confirmed that the emission intensities from single PSIs show roughly linear dependence on excitation powers, at least below 40 μW, as shown in Fig. 6. Therefore, we conclude that the effect of annihilation is not serious in the present experiment. Elli et al. also studied the excitation-power dependence of single PSI fluorescence [24]. Their data, showing linearity up to ca. $5\ \text{kW/cm}^2$, is consistent with our result if we take into account that our experiments were done with a 633-nm excitation laser where the absorbance of Chl is ca. 10% of that of the 672-nm excitation laser used by Elli et al. Fig. 6A also shows that the coefficient of variation, the degree of blinking, does not show noticeable dependence on the excitation power. From this observation, we consider that the conformation fluctuation inducing the observed blinking is not light dependent: the effect of local heating or the interaction of amino acid residues with the excited Chl is not involved in the mechanism of the blinking.

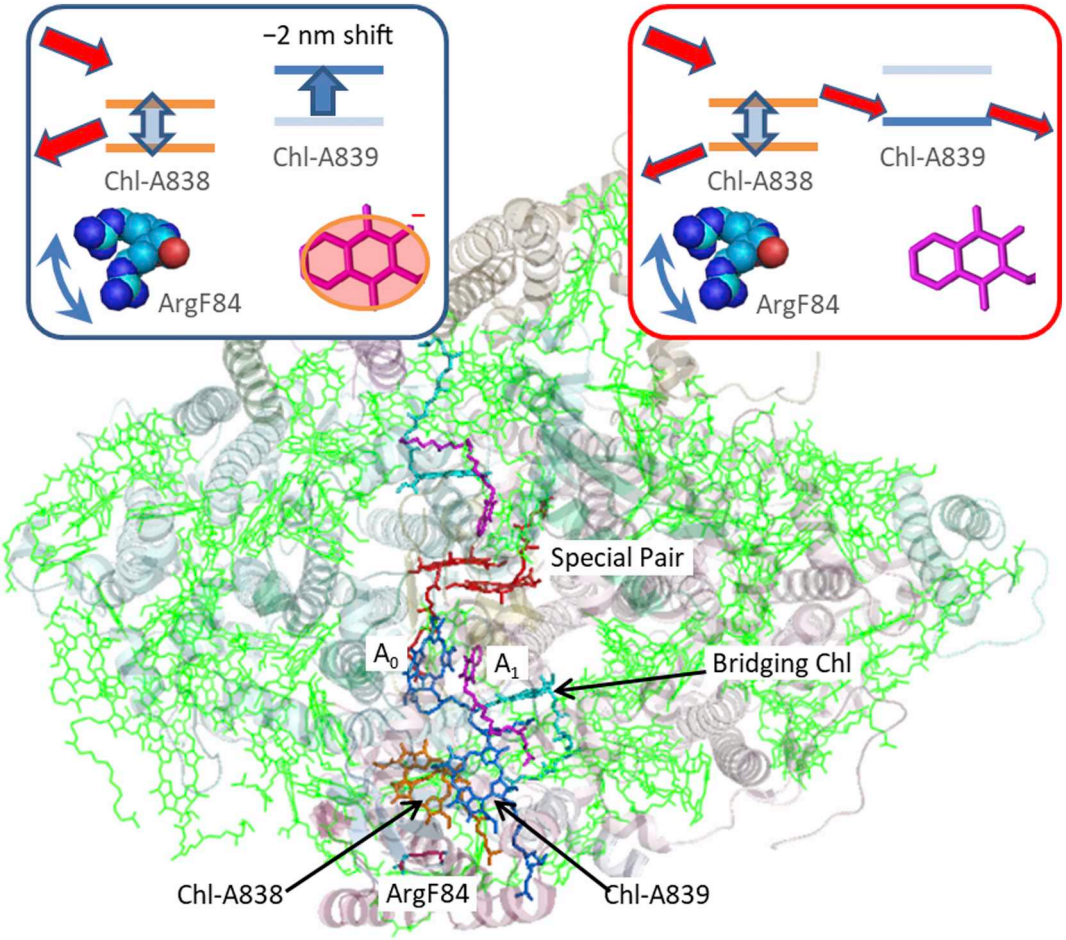

Fig. 7. Bottom: co-factor arrangement in the *Synecocystis* PSI structure (PDB entry: 5OY0). The co-factors and arginine F84 relevant to the proposed model of the blinking are depicted in thick lines in red (special pair), blue (A_0 and Chl-A839 with large ESs), cyan (bridging Chl), orange (Chl-A838), and in magenta (phylloquinones). The other Chls are depicted in thin green lines. Top: schematic description of the model of the variable excitation-energy path due to the site energy changes of Chls-A838 (orange horizontal lines) and A839 (blue horizontal lines) upon conformation fluctuation of ArgF84 and one-electron reduction of A_1, respectively. Red arrows indicate the directions of the preferred excitation-energy flow. (For interpretation of the references to color in this figure legend, the reader is referred to the web version of this article.)

5. Conclusion

We investigated here the intermittent fluctuation in the emission intensities of single PSIs. The temporal variations in the emission intensities were attributed to alterations in the energy-transfer pathway within the PSI trimer, which in turn change the redistribution ratios of excitons between the terminal emitter, C714, and the quencher, $P700^+$. The small fluctuations in the fluorescence peak positions at 80 K are in marked contrast to those reported for another pigment-binding protein, like myoglobin, which showed a roughly 100 cm^{-1} shift of the transient hole-burning spectrum at even higher temperatures, above 200 K [49]. We proposed a tentative model explaining the mechanism for the blinking. In the model, we assumed that the fluctuation in the site energy of Chl-A838 near the bridging Chl disturbs the energy distribution ratio between $P700^+$, as the quencher, and the red Chl, as the emitter. We found that Chl-A839 adjacent to A838 has a large ES upon the phylloquinone redox-state change. The pair of Chls, Chl-A838 and A839, may be involved in the modified blinking property by the pre-oxidation of P700. The physiological relevance of the observed blinking is not clear at present. As suggested by Brecht et al. [28], it may contribute to the photostability of antenna Chls in PSI by making them evenly excited.

Transparency document

The Transparency document associated with this article can be found, in online version.

Acknowledgments

This work was supported in part by JSPS KAKENHI Grant Numbers JP21750017 and JP24370060 to Y.S., JP15F15032 to S. J., and JP17H06435 and JP17H03662 to T. N.

Appendix A. Supplementary data

Supplementary data to this article can be found online at https://doi.org/10.1016/j.bbabio.2018.11.002.

References

[1] M. Brecht, H. Studier, V. Radics, J.B. Nieder, R. Bittl, Spectral diffusion induced by proton dynamics in pigment-protein complexes, J. Am. Chem. Soc. 130 (2008) 17487–17493.
[2] T.P.J. Krüger, E. Wientjes, R. Croce, R. van Grondelle, Conformational switching

explains the intrinsic multifunctionality of plant light-harvesting complexes, Proc. Natl. Acad. Sci. U. S. A. 108 (2011) 13516–13521.
[3] T. Kondo, A. Pinnola, W.J. Chen, L. Dall'Osto, R. Bassi, G.S. Schlau-Cohen, Single-molecule spectroscopy of LHCSR1 protein dynamics identifies two distinct states responsible for multi-timescale photosynthetic photoprotection, Nat. Chem. 9 (2017) 772–778.
[4] P. Jordan, P. Fromme, H.T. Witt, O. Klukas, W. Saenger, N. Krauβ, Three-dimensional structure of cyanobacterial photosystem I at 2.5 angstrom resolution, Nature 411 (2001) 909–917.
[5] X.C. Qin, M. Suga, T.Y. Kuang, J.R. Shen, Structural basis for energy transfer pathways in the plant PSI-LHCI supercomplex, Science 348 (2015) 989–995.
[6] T. Malavath, I. Caspy, S.Y. Netzer-EI, D. Klaiman, N. Nelson, Structure and function of wild-type and subunit-depleted photosystem I in *Synechocystis*, Biochim. Biophys. Acta, Bioenerg. 1859 (2018) 645–654.
[7] M. Watanabe, H. Kubota, H. Wada, R. Narikawa, M. Ikeuchi, Novel supercomplex organization of photosystem I in *Anabaena* and *Cyanophora paradoxa*, Plant Cell Physiol. 52 (2011) 162–168.
[8] M. Li, D.A. Semchonok, E.J. Boekema, B.D. Bruce, Characterization and evolution of tetrameric photosystem I from the thermophilic cyanobacterium *Chroococcidiopsis* sp TS-821, Plant Cell 26 (2014) 1230–1245.
[9] V.V. Shubin, S.D.S. Murthy, N.V. Karapetyan, P. Mohanty, Origin of the 77-K variable fluorescence at 758-nm in the cyanobacterium *Spirulina-Platensis*, Biochim. Biophys. Acta 1060 (1991) 28–36.
[10] N.V. Karapetyan, Protective dissipation of excess absorbed energy by photosynthetic apparatus of cyanobacteria: role of antenna terminal emitters, Photosynth. Res. 97 (2008) 195–204.
[11] E. Schlodder, M. Hussels, M. Çetin, N.V. Karapetyan, M. Brecht, Fluorescence of the various red antenna states in photosystem I complexes from cyanobacteria is affected differently by the redox state of P700, Biochim. Biophys. Acta, Bioenerg. 1807 (2011) 1423–1431.
[12] L.O. Pålsson, J.P. Dekker, E. Schlodder, R. Monshouwer, R. van Grondelle, Polarized site-selective fluorescence spectroscopy of the long-wavelength emitting chlorophylls in isolated photosystem I particles of *Synechococcus elongatus*, Photosynth. Res. 48 (1996) 239–246.
[13] M. Rätsep, T.W. Johnson, P.R. Chitnis, G.J. Small, The red-absorbing chlorophyll a antenna states of photosystem I: a hole-burning study of *Synechocystis* sp PCC 6803 and its mutants, J. Phys. Chem. B 104 (2000) 836–847.
[14] V. Zazubovich, S. Matsuzaki, T.W. Johnson, J.M. Hayes, P.R. Chitnis, G.J. Small, Red antenna states of photosystem I from cyanobacterium *Synechococcus elongatus*: a spectral hole burning study, Chem. Phys. 275 (2002) 47–59.
[15] E. Schlodder, F. Lendzian, J. Meyer, M. Çetin, M. Brecht, T. Renger, N.V. Karapetyan, Long-wavelength limit of photochemical energy conversion in photosystem I, J. Am. Chem. Soc. 136 (2014) 3904–3918.
[16] C. Slavov, M. Reus, A.R. Holzwarth, Two different mechanisms cooperate in the desiccation-induced excited state quenching in Parmelia Lichen, J. Phys. Chem. B 117 (2013) 11326–11336.
[17] N.V. Karapetyan, Y.V. Bolychevtseva, N.P. Yurina, I.V. Terekhova, V.V. Shubin, M. Brecht, Long-wavelength chlorophylls in photosystem I of cyanobacteria: origin, localization, and functions, Biochem. Mosc. 79 (2014) 213–220.
[18] Y. Shibata, A. Mohamed, K. Taniyama, K. Kanatani, M. Kosugi, H. Fukumura, Red shift in the spectrum of a chlorophyll species is essential for the drought-induced dissipation of excess light energy in a poikilohydric moss, *Bryum argenteum*, Photosynth. Res. 136 (2018) 229–243.
[19] T. Hiyama, B. Ke, Difference spectra and extinction coefficients of P700, Biochim. Biophys. Acta 267 (1972) 160–171.
[20] M.S. Davis, A. Forman, J. Fajer, Ligated chlorophyll cation radicals - their function in photosystem-ii of plant photosynthesis, Proc. Natl. Acad. Sci. U. S. A. 76 (1979) 4170–4174.
[21] E. Schlodder, M. Çetin, M. Byrdin, I.V. Terekhova, N.V. Karapetyan, P700(+)- and (3)P700-induced quenching of the fluorescence at 760 nm in trimeric Photosystem I complexes from the cyanobactenium Arthrospira platensis, Biochim. Biophys. Acta, Bioenerg. 1706 (2005) 53–67.
[22] M. Brecht, M. Hussels, E. Schlodder, N.V. Karapetyan, Red antenna states of Photosystem I trimers from *Arthrospira platensis* revealed by single-molecule spectroscopy, Biochim. Biophys. Acta, Bioenerg. 1817 (2012) 445–452.
[23] F. Jelezko, C. Tietz, U. Gerken, J. Wrachtrup, R. Bittl, Single-molecule spectroscopy on photosystem I pigment-protein complexes, J. Phys. Chem. B 104 (2000) 8093–8096.
[24] A.F. Elli, F. Jelezko, C. Tietz, H. Studier, M. Brecht, R. Bittl, J. Wrachtrup, Red pool chlorophylls of photosystem I of the cyanobacterium *Thermosynechococcus elongatus*: a single-molecule study, Biochemistry 45 (2006) 1454–1458.
[25] K.J. Riley, T. Reinot, R. Jankowiak, P. Fromme, V. Zazubovich, Red antenna states of photosystem I from cyanobacteria *Synechocystis* PCC 6803 and *Thermosynechococcus elongatus*: single-complex spectroscopy and spectral hole-burning study, J. Phys. Chem. B 111 (2007) 286–292.
[26] M. Brecht, H. Studier, A.F. Elli, F. Jelezko, R. Bittl, Assignment of red antenna states in photosystem I from *Thermosynechoccocus elongatus* by single-molecule spectroscopy, Biochemistry 46 (2007) 799–806.
[27] M. Brecht, V. Radics, J.B. Nieder, H. Studier, R. Bittl, Red antenna states of photosystem I from *Synechocystis* PCC 6803, Biochemistry 47 (2008) 5536–5543.
[28] M. Brecht, V. Radics, J.B. Nieder, R. Bittl, Protein dynamics-induced variation of excitation energy transfer pathways, Proc. Natl. Acad. Sci. U. S. A. 106 (2009) 11857–11861.
[29] M. Hussels, M. Brecht, Effect of glycerol and PVA on the conformation of photosystem I, Biochemistry 50 (2011) 3628–3637.
[30] H. Frauenfelder, S.G. Sligar, P.G. Wolynes, The energy landscapes and motions of proteins, Science 254 (1991) 1598–1603.
[31] H. Frauenfelder, P.G. Wolynes, R.H. Austin, Biological physics, Rev. Mod. Phys. 71 (1999) S419–S430.
[32] C. Hofmann, H. Michel, M. van Heel, J. Kohler, Multivariate analysis of single-molecule spectra: Surpassing spectral diffusion, Phys. Rev. Lett. 94 (2005) 195501.
[33] Y. Shibata, W. Katoh, T. Chiba, K. Namie, N. Ohnishi, J. Minagawa, H. Nakanishi, T. Noguchi, H. Fukumura, Development of a novel cryogenic microscope with numerical aperture of 0.9 and its application to photosynthesis research, Biochim. Biophys. Acta, Bioenerg. 1837 (2014) 880–887.
[34] R. Nagao, M. Yamaguchi, S. Nakamura, H. Ueoka-Nakanishi, T. Noguchi, Genetically introduced hydrogen bond interactions reveal an asymmetric charge distribution on the radical cation of the special-pair chlorophyll P680, J. Biol. Chem. 292 (2017) 7474–7486.
[35] E. Schlodder, K. Falkenberg, M. Gergeleit, K. Brettel, Temperature dependence of forward and reverse electron transfer from A(1)(−), the reduced secondary electron acceptor in photosystem I, Biochemistry 37 (1998) 9466–9476.
[36] P. Setif, H. Bottin, Identification of Electron-transfer reactions involving the acceptor-A1 of photosystem-I at room-temperature, Biochemistry 28 (1989) 2689–2697.
[37] F. Müh, M. Plöckinger, T. Renger, Electrostatic asymmetry in the reaction Center of Photosystem II, J. Phys. Chem. Lett. 8 (2017) 850–858.
[38] S. Krawczyk, Electrochromism of chlorophyll-*a* monomer and special pair dimer, Biochim. Biophys. Acta 1056 (1991) 64–70.
[39] R.N. Frese, M.A. Palacios, A. Azzizi, I.H.M. van Stokkum, J. Kruip, M. Rögner, N.V. Karapetyan, E. Schlodder, R. van Grondelle, J.P. Dekker, Electric field effects on red chlorophylls, beta-carotenes and P700 in cyanobacterial Photosystem I complexes, Biochim. Biophys. Acta, Bioenerg. 1554 (2002) 180–191.
[40] J.M. Sevilla, M. Dominguez, F. Garciablanco, M. Blazquez, Resolution of absorption-spectra, Comput. Chem. 13 (1989) 197–200.
[41] Y. Shibata, Y. Saga, H. Tamiaki, S. Itoh, Low-temperature fluorescence from single chlorosomes, photosynthetic antenna complexes of green filamentous and sulfur bacteria, Biophys. J. 91 (2006) 3787–3796.
[42] J.M. Hayes, S. Matsuzaki, M. Rätsep, G.J. Small, Red chlorophyll a antenna states of photosystem I of the cyanobacterium *Synechocystis* sp PCC 6803, J. Phys. Chem. B 104 (2000) 5625–5633.
[43] J. Pieper, M. Rätsep, R. Jankowiak, K.D. Irrgang, J. Voigt, G. Renger, G.J. Small, Q(y)-level structure and dynamics of solubilized light-harvesting complex II of green plants: pressure and hole burning studies, J. Phys. Chem. A 103 (1999) 2412–2421.
[44] M.L. Groot, R.N. Frese, F.L. de Weerd, K. Bromek, Å. Pettersson, E.J.G. Peterman, I.H.M. van Stokkum, R. van Grondelle, J.P. Dekker, Spectroscopic properties of the CP43 core antenna protein of photosystem II, Biophys. J. 77 (1999) 3328–3340.
[45] J. Adolphs, F. Müh, M.E.A. Madjet, M.S.A. Busch, T. Renger, Structure-based calculations of optical spectra of photosystem I suggest an asymmetric light-harvesting process, J. Am. Chem. Soc. 132 (2010) 3331–3343.
[46] M. Byrdin, I. Rimke, E. Schlodder, D. Stehlik, T.A. Roelofs, Decay kinetics and quantum yields of fluorescence in photosystem I from *Synechococcus elongatus* with P700 in the reduced and oxidized state: are the kinetics of excited state decay trap-limited or transfer-limited? Biophys. J. 79 (2000) 992–1007.
[47] Y. Shibata, A. Yamagishi, S. Kawamoto, T. Noji, S. Itoh, Kinetically distinct three red chlorophylls in photosystem I of *Thermosynechococcus elongatus* revealed by femtosecond time-resolved fluorescence spectroscopy at 15 K, J. Phys. Chem. B 114 (2010) 2954–2963.
[48] S. Cazzaniga, M. Bressan, D. Carbonera, A. Agostini, L. Dall'Osto, Differential roles of carotenes and xanthophylls in photosystem I Photoprotection, Biochemistry 55 (2016) 3636–3649.
[49] Y. Shibata, A. Kurita, T. Kushida, Real-time observation of conformational fluctuations in Zn-substituted myoglobin by time-resolved transient hole-burning spectroscopy, Biophys. J. 75 (1998) 521–527.